PAPER Nr. : 44

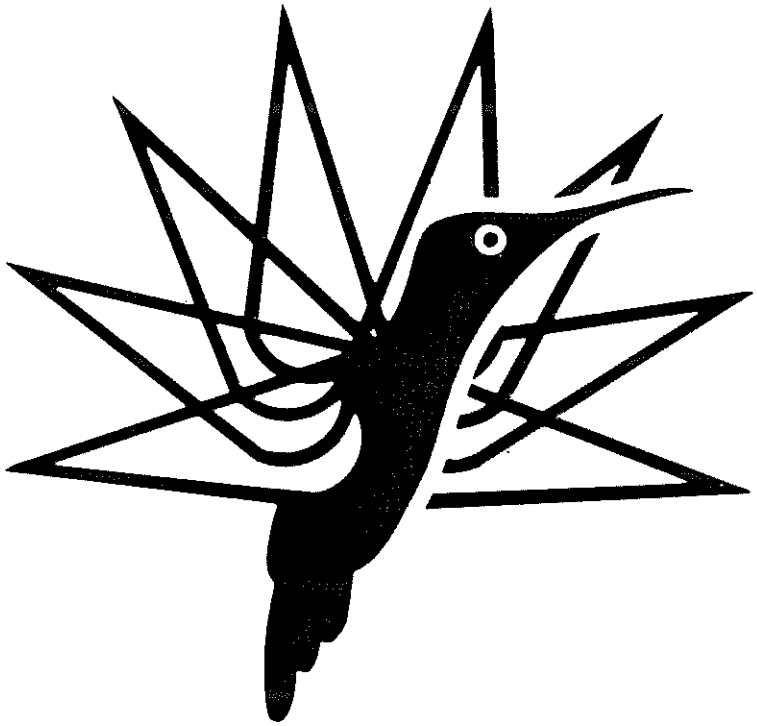

USE OF AN OPTIMIZED CONTROLLER AND A FINITE-STATE STALL MODEL TO FIND TRIMMED HELICOPTER FLIGHT CONTROLS

BY

DAVID A. PETERS
MNAOUAR CHOUCHANE
MARK FULTON

SCHOOL OF AEROSPACE ENGINEERING
GEORGIA INSTITUTE OF TECHNOLOGY
ATLANTA, GEORGIA, U.S.A

FIFTEENTH EUROPEAN ROTORCRAFT FORUM

SEPTEMBER 12 - 15, 1989 AMSTERDAM

Use of an Optimized Controller and a Finite-State Stall Model to Find Trimmed Helicopter Flight Controls

by

David A. Peters
Professor

and

Mnaouar Chouchane Mark Fulton
Research Assistants

School of Aerospace Engineering
Georgia Institute of Technology
Atlanta, GA 30332, USA

Abstract

An auto-pilot is applied to helicopter rotor flap-lag-torsion equations in order to obtain the control settings for a trimmed flight condition. The rotor aerodynamic description includes a state-space dynamic stall model for lift and for pitching moments. Thus, we attempt to trim the rotor for flight conditions in which significant stall and torsional deformations are present. The auto-pilot is extended to Q-bladed rotors by a series of time-delay terms. As a result, the optimum gains and time constants depend upon the number of blades as well as upon the torsional stiffness.

List of Symbols

a	slope of the airfoil lift curve, $(/rad)$
b	blade semi-chord, $c/2$
$\bar{b}$	nondimensionlized blade semi-chord, b/R
c	blade chord, m
$\bar{c}$	nondimensionlized blade chord, c/R
C_D	drag force coefficient, $D/\pi R^2\rho\Omega^2R^2$
C_L	hub roll moment coefficient, $L/\pi R^2\rho\Omega^2R^2$
$\bar{C}_L$	normalized roll moment coefficient, $C_L/\sigma a$
C_M	pitch moment coefficient, $M/\pi R^3\rho\Omega^2R^2$
$\bar{C}_M$	normalized pitch moment coefficient, $C_M/\sigma a$
C_T	blade thrust coefficient, $T/\pi R^2\rho\Omega^2R^2$
$\bar{C}_T$	normalized blade thrust coefficient, $C_L/\sigma a$
C_z	lift coefficient, $\bar{L}/U^2$
C_ζ	Rayleigh damping coefficient
D	airfoil profile drag per unit length, N/m
$\bar{e}$	aerodynamic center offset divided by chord
e_A	distance between shear center and center of airfoil area
E	Young's modulus, N/m^2
$\bar{f}$	flat plate drag area divided by πR^2
F_x, F_y	aerodynamic forces per unit length in the deformed blade, N/m
$I_{y'}, I_{z'}$	cross-sectional area moment of inertia, m^4
J	torsional rigidity constant, m^4

k_m	blade cross-section radius of gyration, m
K_β	stiffness of flap root spring, Nm/rad
K_ϕ	stiffness of torsional root spring, Nm/rad
K_ζ	stiffness of lag root spring, Nm/rad
L	aerodynamic lift per unit length, N/m
$\bar{L}$	lift per unit length divided by $\rho\Omega^2R^3$
L_α, L_N	circualtory and noncirculatory lift, respectively, N/m
m	mass per unit length of the blade, kg/m
M_ϕ	generalized aerodynamic moment per unit length, mN/m
p	dimensionless rotating flapping frequency, $\sqrt{1+K_\beta/\Omega^2 I_x}$
r	distance from hub center, m
R	blade length, m
s	apparent mass coefficient
t	time, sec
$\bar{t}$	nondimensional time, Ωt
U	blade airfoil velocity with respect to air, m/sec
u , v, w	elastic deformations in x, y, z directions respectively, m
$\bar{u}$, $\bar{v}$, $\bar{w}$	nondimensional elastic deformations, $(u,v,w)/R$
V_i	induced downwash velocity, m/sec
$V(\bar{x})$, $W(\bar{x})$	comparison functions for bending
x, y, z	inertial coordinate system for undeformed blade, m
x', y', z'	inertial coordinate system for the deformed blade
β	rigid blade flap angle, rad
γ	Lock number
$\bar{\Gamma}$	nondimensional circulation, $\bar{L}/U$
ϵ	scaling parameter in the ordering scheme, (=.1)
Λ_1	nondimensional parameter, $EI_{z'}/m\Omega^2R^4$
Λ_2	nondimensional parameter, $EI_{y'}/m\Omega^2R^4$
Λ_3	nondimensional parameter, $G/m\Omega^2$
Λ_4	nondimensional radial stiffness, $AE/m\Omega^2R^2$
μ	advance ratio
Ω	rotor blade anglular velocity, rad/sec
θ	blade pitch angle, rad
θ_0, θ_s, θ_c	collective and cyclic pitch angles, rad
ρ	air density, Kg/m^3
σ	rotor solidity, $c/\pi r$
ϕ	torsional deflection, rad
ψ	rotor azimuth angle, $\psi = \Omega t$
ζ	rigid blade lag angle, rad
$(\ )_x$, $(\ )_y$	x and y components
$\dot{(\ )}$	$\partial(\ )/\partial t$
$(\ )'$	$\partial(\ )/\partial x$
$(\ )^+$	$\partial(\ )/\partial\bar{x} = \frac{1}{R}\partial(\ )/\partial x$
$\overset{*}{(\ )}$	$\partial(\ )/\partial\bar{t} = \frac{1}{\Omega}\partial(\ )/\partial t$
$(\ )_1$,$(\ )_2$	unstalled, stalled contributions.

1 Introduction

Computation of the vibrations and stability of rotary-wing aircraft in forward flight requires finding a periodic solution to a set of nonlinear, time-varying, partial differential equations. This, in itself, can be a formidable task because the periodic solution may be very lightly damped or even unstable. Therefore, conventional time-marching is not always satisfactory. However, whether the periodic solution is stable or unstable, the computation is made even more difficult by the fact that the equations contain unknown trim parameters (such as pilot control settings, airframe orientation angles, etc.) which must be chosen such that the final periodic solution satisfies the trim-equilibrium equations of a given flight condition. Thus, the rotary-wing analyst is faced with the solution of nonlinear equations with integral constraints on the solution. The solution of this constrained problem stands as one of the most difficult obstacles to analysis of rotary-wing aircraft with many degrees of freedom.

Presently, there are many proposed solution methodologies for this problem. Each has its strengths and weaknesses. For the time-wise solution, there are three general categories of methods. First, there are time-marching algorithms, including conventional methods as well as finite-elements in time, Ref. [1]. Second, there are harmonic-balance techniques of various types, Ref. [2]. Third, there are transition-matrix methods including convolution, Ref. [3], and periodic shooting, Ref. [4]. For the solution of the trim constraints, there are also several alternatives. First, there is Newton-Raphson iteration on the control variables (which involves a complete periodic solution for each control perturbation). Second, there are closed-form force-balance equations which can be used as constraint equations to be solved in paralled with the other equations, Ref. [5]. Third, there are auto-pilots which "fly" the rotor to trim during the time-marching towards a periodic solution, Ref. [6].

Once a periodic, trimmed equilibrium has been found, the dynamicist must find the dynamic behavior of perturbations away from this periodic orbit. This is often complicated by the fact that the aerodynamic models utilized in the equations either have hidden dynamic states or else have an infinite number of dynamic states (due to time delays, lift-deficiency functions, ets.) Furthermore, many of the trim methodologies (such as transition-matrix methods or periodic shooting) also require explicit knowledge of these states. Therefore, another challenge for the analyst is to develop aerodynamic theories that have explicit states. To this end, several researchers have investigated state-variable wake models, Ref. [7-9]; and others have investigated finite-state lift models that include dynamic stall, Ref. [10-13].

In this paper, we explore trimming by the auto-pilot method. The auto-pilot method is not appropriate near blade stability boundaries. However, it is very efficient for well-damped rotors with many degrees of freedom and with complicated aerodynamics. In the past, however, its deficiency has been that a user would not know *a priori* what gains, time constants, and couplings to use. Those optimized in hover, for example, often failed in forward flight. One purpose of this paper is to improve those controllers. The rotor equations include flap, lag, and torsion; and they include the dynamic stall model of Ref. [12]. In addition, the present work includes state variables that describe the unsteady pitching moments. The existing auto-pilot equations, although previously optimized for simple linear flapping, have never been applied successfully to flap-lag-torsion in forward flight with high thrust and significant stall. Therefore, we have reformulated the auto-pilot and re-optimized it for these more stringent conditions. This paper describes the results of this reformulation on rotor trimming. The work is an extension of that found in Ref. [14].

2 Mathematical Model of Rotor

2.1 Structural Model

We present here the vertical and inplane bending equations and the torsion equation. The nondimensional form is obtained by dividing both sides of the dimensional form of each equation by $m\Omega^2 R$. Terms including blade precone are not considered here. The derivation and a more extensive discussion related to these equations can be found in Ref. [15]. Only terms of order ϵ and ϵ^3 are retained in the nondimensional flap equation.

$$-(\tau\overline{w}^{+})^{+}+(\Lambda_1-\Lambda_2)(\theta+\phi)\overline{v}^{++++}+\{\Lambda_2+(\Lambda_1-\Lambda_2)(\theta+\phi)^2\}\overline{w}^{++++}+\overset{**}{\overline{w}}=\overline{L}_w \quad (1)$$

where τ is the nondimensional tension expressed as

$$\tau(1,\epsilon^2)=\frac{1-x^2}{2}+\int_{\bar{x}}^{1}(2\overset{*}{\bar{v}}+\bar{u}-\overset{**}{\bar{u}}+\bar{L}_u)d\bar{x} \quad (2)$$

In the lag equation, terms of order ϵ^2 and ϵ^4 are retained:

$$-(\tau\overline{v}^{+})^{+}+\{\Lambda_1+(\Lambda_2-\Lambda_1)(\theta+\phi)^2\}\overline{v}^{++++}+(\Lambda_1-\Lambda_2)(\theta+\phi)\overline{w}^{++++}+2\overset{*}{\overline{u}}+\overset{**}{\overline{v}}-\overline{v}=\overline{L}_v \quad (3)$$

where,

$$\overset{*}{\bar{u}}=-\int_0^{\bar{x}}\overline{w}^{+}\overset{*}{\bar{w}}^{+}d\bar{x} \quad (4)$$

The torsion equation is written in a nondimensional form with terms of order (ϵ^4)

$$-\Lambda_3 J\phi^{++}+\bar{e}\{\overline{xw}^{+}+\overset{**}{\bar{w}}\}-\bar{e}_A\overline{w}^{++}\Lambda_4(\overline{u}^{+}+\frac{\overline{w}^{+2}}{2})=\overline{M}_\phi \quad (5)$$

The generalized aerodynamic forces per unit length in the inertial reference system L_v and L_w are expressed in terms of L_x and L_y, the aerodynamic forces per unit length in the deformed blade coordinates. They are expressed in a nondimensional form as follows

$$\overline{L}_v=-\{\overline{L}_x\cos(\theta+\phi)+\overline{L}_y\sin(\theta+\phi)\} \quad (6)$$

$$\overline{L}_w=\{-\overline{L}_x\sin(\theta+\phi)+\overline{L}_y\cos(\theta+\phi)\} \quad (7)$$

The above equations have been compared in Ref. [15] with other work related to blade equations. When the equations are written to the higher order, they include all the terms of the equations derived by other authors and more. This is due to the assumptions and the method used in the derivation, in addition to the scaling procedure.

2.2 Unified Lift Model

The unified lift model extends the ONERA model to include plunge, unsteady free stream, and large angles of attack. In the modification, a distinction is made between the angle of attack due to pitch motion and that due to plunging motion. Furthermore, the unified model separates the apparent-mass lift, $\bar{L}_0$, from the circulatory lift. Thus, we have, for the components of lift normal to the chord (L_y) and along the chord (L_x), Fig. 1.

$$\bar{L}_y=\bar{L}_0+U_x(\bar{\Gamma}_1+\bar{\Gamma}_2) \quad (8)$$

$$\bar{L}_x=-U_y(\bar{\Gamma}_1+\bar{\Gamma}_2) \quad (9)$$

where,

$$\bar{L}_0=\bar{b}s\overset{*}{\bar{U}}_y \quad (10)$$

Table 1: Identified Coefficients of Stall Equations

Parameter	Numerical Value	Physical Description
λ	0.2	time delay parameter
s	$5\pi/180$	apparent mass quantity
$\bar{\delta}$	$(\frac{\partial C_z}{\partial \alpha} - \frac{4\pi}{180})(1 + 1.43\Delta C_z)$	relates lift coefficient to the pitch rate
w	$0.10 + 0.023(\lvert\alpha\rvert - 13^0)u(\lvert\alpha\rvert - 13^0)$ $\lvert\alpha\rvert < 21.7$ $0.3 \quad \lvert\alpha\rvert > 21.7$	a damping factor
d	$0.105/w$	stall natural frequency
e	$2 - 5.1\tan^{-1}\{1.21(\lvert\alpha\rvert - 13^0)\}u(\lvert\alpha\rvert - 13^0)$	phase shift parameter

and where U_x and U_y are the components of the flow along the chord and normal to the chord (respectively). The unified model has the same structure as the Greenberg and Theodorsen theories at small angles of attack. A complete discussion of the refinement which led to the unified model is presented in Ref. [12]. The simplified version, in which reversed flow is approximated and higher order terms in $\overline{\Gamma}_2$ equation are neglected, is

$$\overline{k}\dot{\overline{\Gamma}}_1 + \lambda\overline{\Gamma}_1 = \lambda a U_y + \delta\dot{\overline{b}}\dot{\epsilon} \tag{11}$$

$$\overline{k}^2\ddot{\overline{\Gamma}}_2 + 2dw\overline{k}\dot{\overline{\Gamma}}_2 + w^2(1+d^2)\overline{\Gamma}_2 = -w^2(1+d^2)\{U_x\Delta C_z + e\overline{k}(\dot{U}_x\Delta C_z + \frac{\partial \Delta C_z}{\partial \alpha}\dot{U}_y)\} \tag{12}$$

where U_x and U_y are normal and chordwise airflow relative to the airfoil and $\overline{k}$ is an average of the reduced frequency of the freestream. The coefficients δ, w, d, e, are evaluated at the instantaneous angle of attack, $\alpha = \tan^{-1}(U_y/U_x)$; and $\dot{\epsilon}$ is the rotation of the airfoil with respect to the air mass. This model is used in the present research work to determine the aerodynamic forces applied on the blade. Although it does not present a perfect representation of the aerodynamic environment in stall regime, it has been shown to give good agreement with experiments and it is certainly more reasonable than the linear, quasi-steady theory presently used in stability analyses.

2.3 Stall coefficients

In the above equations, the total circulation density Γ is expressed as a sum of two components, Γ_1 and Γ_2. Γ_1 is the circulation density associated with a linear model. Γ_2, however, is the deviation of the circulation from the linear value due to stall. The model is expressed by differential equations which depend on ΔC_z, which is the difference between the linear static lift coefficient ($C_{zl} = a\sin\alpha$) and the actual stalled lift coefficient C_{zs}.

The coefficients λ, a, s, δ, d, w, and e depend on the angle of attack only. In Table 1, we present, for illustrative purposes, the numerical values of these coefficients determined by wind tunnel tests and parameter identification for an OA212 airfoil. In this table, u is the unit step function. It is equal to unity for a positive argument and zero otherwise.

The static lift curve for a typical airfoil is presented in Fig. 2. The lift coefficient is linear between -10^0 and 10^0. For large angles, the magnitude shows a deviation from

linearity. C_{zl} is the static coefficient extrapolated from the linear region. C_{zs} is the actual static lift. In the unified lift model of Ref. [12], the linear component of the circulation with reversed flow is expressed as $\Gamma_l = aU \sin\alpha \cos\alpha$ where, for the OA212 airfoil, $a = 7.1$.

2.4 Aerodynamic Pitching Moment Model

The pitching moment per unit length about the aerodynamic center, positive nose up, is expressed in Ref. [11]. The nondimensional version is given by

$$\bar{M}_\phi = \frac{1}{6}\frac{\gamma\bar{c}}{a}[U^2 C_{ml} + U^2 C_{m2} + c_1\bar{b}\dot{\bar{U}}_y + c_2\bar{b}U\dot{\bar{\epsilon}} + c_3\bar{b}^2(\ddot{\bar{\theta}} + \ddot{\bar{\phi}})] \tag{13}$$

In the above equation, C_{ml} is the linear static moment coefficient, C_{m2} is the nonlinear component of the pitching moment due to stall. θ is the pitch angle, and ϕ is the elastic angle. The coefficients c_1, c_2, and c_3, are empirical coefficients which depend on the Mach number and which have been found to have the following expressions for the OA212 airfoil

$$c_1 = -\frac{\pi}{4}(1 + 1.4M^2) \tag{14}$$

$$c_2 = c_1 \tag{15}$$

$$c_3 = -\frac{3\pi}{16}[-1.26 - 1.53\arctan(15(M - 0.7))] \tag{16}$$

The effect of the airfoil geometry on the pitching moment due to unstalled flow is included through the C_{ml} coefficient only.

The curves of the actual static moment coefficient C_{ms} and its linear counterpart C_{ml} for an OA212 airfoil are presented in Fig. 3. It is important to mention that this curve is accurate for small positive angles of attack ($0 \leq \alpha \leq 25^0$). The extension of the curve for other angles is approximate. This extension was guided by typical airfoil test data. For large angles of attack and in the reversed flow regime, the goal is to use a well-behaved approximation of the static coefficients since the angle of attack of any blade section more often falls in the range of small or moderate angles ($0 \leq \alpha \leq 25^0$).

The nonlinear moment coefficient C_{m2} is computed from the following expression

$$\bar{k}^2\ddot{C}_{m2} + a\bar{k}\dot{C}_{m2} + rC_{m2} = -rU\Delta C_m + E\bar{k}\dot{\bar{U}}_y \tag{17}$$

The coefficients of the C_{m2} equation were found to have common forms for a variety of aifoils. Each coefficient depends on the geometry of the airfoil and on ΔC_z, the difference between the actual static lift coefficient and its linear counterpart. These coefficients have the following expressions

$$r = (r_0 + r_2\Delta C_z^2) \tag{18}$$

$$a = a_0 + a_2\Delta C_z^2 \tag{19}$$

$$E = E_2\Delta C_z^2 \tag{20}$$

It can be noted that the C_{m2} coefficient is equal to zero when the flow is not stalled. This is due to the fact that ΔC_m and E are both equal to zero for this case. Table 2 provides the order of terms in the pitching moment equation.

Table 2: Scaling of the Terms of the Moment Equation

Parameter	Value or Expression	Assumed Order
U	$U \approx U_x(1, \epsilon^2)$	1
C_{m1}	$-.08 \rightarrow .08$	ϵ
C_{m2}		1
c_1	$c_1 \approx -\pi/4$	1
c_2	$c_2 \approx c_1$	1
c_3	$c_3 \approx -3\pi/16$	1
$\bar{b}$		1
$\overset{*}{\theta}$		ϵ
$\gamma\bar{c}/6a$	$\approx .02$	ϵ^2
$U^2 C_{m1}$		ϵ^2
$U^2 C_{m2}$		ϵ^2
$c_1 \bar{b} \overset{*}{U}_y$		ϵ^2
$c_2 \bar{U} \overset{*}{\epsilon}$		ϵ^2
$c_3 \bar{b}^2 \overset{**}{\alpha}$		ϵ^4

3 Auto-Pilot Equations

3.1 Trim Formulation

Any flight vehicle should be able to maintain equilibrium during steady flight conditions. This means that the resultant forces and moments on the aircraft are equal to zero. In a fixed-wing aircraft, external aerodynamic control surfaces (such as ailerons, elevators, and rudders) perform this function.

In a helicopter, trim is performed by variation of blade angle as a function of the azimuth angle of the blade so that rolling and pitching of the aircraft is avoided. This is accomplished through pilot-controlled inputs of collective pitch (θ_0) and cyclic pitch (θ_s, θ_c). The pitch mechanism produces the pitch setting for a helicopter trimmed condition which is expressed as follows

$$\theta = \theta_0 + \theta_s \sin\psi + \theta_c \cos\psi \tag{21}$$

In the trimmed condition, the rotor is maintained at a fixed thrust coefficient C_T in forward flight. Thus, the trim procedure requires the knowledge of the helicopter control settings as the azimuth angle varies, depending on the flight condition.

3.2 Automatic Feed-Back Controls

One way of trimming the helicopter is to use an automatic feed-back system that would trim the helicopter automatically as the rotor equations are integrated in time. Here, the control settings are assumed unknown. Hence, they are calculated simultaneously along with the generalized coordinates of the blade equations. One possible form of the auto-pilot equations is derived in Ref. [6]. These equations can be

expressed in either of the following two forms

$$\begin{bmatrix} \tau_0 & 0 & 0 \\ 0 & \tau_1 & 0 \\ 0 & 0 & \tau_1 \end{bmatrix} \begin{Bmatrix} \ddot{\theta}_0 \\ \ddot{\theta}_s \\ \ddot{\theta}_c \end{Bmatrix} + \begin{Bmatrix} \dot{\theta}_0 \\ \dot{\theta}_s \\ \dot{\theta}_c \end{Bmatrix} = \begin{bmatrix} K_0 & 0 & 0 \\ 0 & K_1 & 0 \\ 0 & 0 & K_1 \end{bmatrix} \begin{bmatrix} \frac{8p^2}{\gamma} & 0 & 0 \\ 0 & \frac{8(p^2-1)}{\gamma} & -1 \\ 0 & 1 & \frac{8(p^2-1)}{\gamma} \end{bmatrix} \begin{Bmatrix} \Delta\beta_0 \\ \Delta\beta_s \\ \Delta\beta_c \end{Bmatrix} \tag{22}$$

$$\begin{bmatrix} \tau_0 & 0 & 0 \\ 0 & \tau_1 & 0 \\ 0 & 0 & \tau_1 \end{bmatrix} \begin{Bmatrix} \ddot{\theta}_0 \\ \ddot{\theta}_s \\ \ddot{\theta}_c \end{Bmatrix} + \begin{Bmatrix} \dot{\theta}_0 \\ \dot{\theta}_s \\ \dot{\theta}_c \end{Bmatrix} = \begin{bmatrix} K_0 & 0 & 0 \\ 0 & K_1 & 0 \\ 0 & 0 & K_1 \end{bmatrix} \begin{bmatrix} \frac{6}{\sigma a} & 0 & 0 \\ 0 & \frac{-16}{\sigma a} & \frac{2\gamma}{\sigma a(p^2-1)} \\ 0 & \frac{-2\gamma}{\sigma a(p^2-1)} & \frac{-16}{\sigma a} \end{bmatrix} \begin{Bmatrix} \Delta\bar{C}_T \\ \Delta\bar{C}_L \\ \Delta\bar{C}_M \end{Bmatrix} \tag{23}$$

where Δ's represent the error between desired and actual values of flapping angles or hub forces. For rigid-blade flapping, these can be approximated by instantaneous "measurements"

$$\Delta\bar{C}_T = \overline{C}_T - \frac{4}{3}\frac{p^2}{\gamma}\beta \tag{24}$$

$$\Delta\bar{C}_L = \overline{C}_L + \frac{p^2-1}{\gamma}\beta\sin\psi \tag{25}$$

$$\Delta\bar{C}_M = \overline{C}_M + \frac{p^2-1}{\gamma}\beta\cos\psi \tag{26}$$

and

$$\Delta\beta_0 = \frac{3}{4}\frac{\gamma}{p^2}\overline{C}_T - \beta \tag{27}$$

$$\Delta\beta_s = \frac{-2\gamma}{(p^2-1)}\overline{C}_L - 2\beta\sin\psi \tag{28}$$

$$\Delta\beta_c = \frac{-2\gamma}{(p^2-1)}\overline{C}_M - 2\beta\cos\psi \tag{29}$$

This automatic feed-back system is used to provide control to the helicopter for numerical purposes. It adjusts the pitch of the blade to maintain thrust, roll moment, and pitching moment. The parameters K_0 and K_1 are controller gains. The parameters τ_0 and τ_1 are time constants.

Application of the above equations has shown unsatisfactory performance for high advance ratios or high lifting conditions. One explanation for this deficiency can be linked to the hover assumption inherent in the above gains and couplings. A more accurate formulation of the above couplings is found in Ref. [2]. These equations are verified, in the same reference, to give accurate results for response derivatives at low advance ratios. Use of these equations to formulate the coupling of the feed-back controller is expected to expand the range of accurate trimming performance.

In general, the static derivatives between controls and loads can be written in a matrix form as follow

$$\begin{Bmatrix} dC_T \\ dC_L \\ dC_M \end{Bmatrix} = \begin{bmatrix} A \end{bmatrix} \begin{Bmatrix} d\theta_0 \\ d\theta_s \\ d\theta_c \end{Bmatrix} \tag{30}$$

in hover, $\mu = 0$, we have

$$\left[A_0 \right] = \begin{bmatrix} \frac{1}{6} & 0 & 0 \\ 0 & -\frac{C^2}{16(1+C^2)} & \frac{-C}{16(1+C^2)} \\ 0 & \frac{C}{16(1+C^2)} & -\frac{C^2}{16(1+C^2)} \end{bmatrix} \tag{31}$$

and where, $C = \frac{8(p^2-1)}{\gamma}$. These are the couplings implicit in Eqs. (24-25).

The more accurate form of these response derivatives in forward flight is given in Ref. [2] and is

$$\left[A_\mu \right] = \begin{bmatrix} \frac{1}{6}(1+\frac{3}{2}\mu^2) & \frac{2}{9}\mu & 0 \\ -\frac{C}{6}\frac{\mu}{1+C^2}\{C - \frac{\gamma}{16p^2}\} & -\frac{C}{16(1+C^2)}\{C[1+\frac{3}{2}\mu^2] - \frac{2}{9}\mu^2\frac{\gamma}{p^2}\} & -\frac{C}{16(1+C^2)} \\ \frac{C}{6}\frac{\mu}{1+C^2}\{1 + C\frac{\gamma}{16p^2}\} & \frac{C}{16(1+C^2)}\{(1+2\mu^2) + \frac{2}{9}\mu^2 C\frac{\gamma}{p^2}\} & -\frac{C^2}{16(1+C^2)}(1+\frac{\mu^2}{2}) \end{bmatrix} \tag{32}$$

Hence, from the above matrix, a feed-back system can be formed in a similar manner as described previously.

$$\begin{bmatrix} \tau_0 & 0 & 0 \\ 0 & \tau_1 & 0 \\ 0 & 0 & \tau_1 \end{bmatrix} \begin{Bmatrix} \ddot{\theta}_0 \\ \ddot{\theta}_s \\ \ddot{\theta}_c \end{Bmatrix} + \begin{Bmatrix} \dot{\theta}_0 \\ \dot{\theta}_s \\ \dot{\theta}_c \end{Bmatrix} = \begin{bmatrix} K_0 & 0 & 0 \\ 0 & K_1 & 0 \\ 0 & 0 & K_1 \end{bmatrix} \left[A_\mu \right]^{-1} \begin{Bmatrix} \frac{C_T}{\sigma a} - \frac{4}{3}\frac{p^2}{\gamma}\beta \\ \frac{C_L}{\sigma a} + \frac{p^2-1}{\gamma}\beta \sin\psi \\ \frac{C_M}{\sigma a} + \frac{p^2-1}{\gamma}\beta \cos\psi \end{Bmatrix} \tag{33}$$

The above system of equations (33) reduces to equations (23) when the hover assumption is used. This implies the substitution of an advance ratio $\mu = 0$ in the above system.

3.3 Optimized Controller

Past studies to optimize the controller have resulted in a variety of combinations of gains and time constants, each resulting in a minimum settling time of about 5 to 8 rotor revolutions. In those studies, Refs. [6] and [14], settling time was minimized subject to constraints on stability and limits on the oscillations of the final control positions due to higher-harmonic input signals from β. To understand these results, it is useful to write equations for a general controller of the type specified in Eq. (33)

$$\begin{bmatrix} \ddots & \\ & \tau_i \\ & & \ddots \end{bmatrix} \begin{Bmatrix} \vdots \\ \ddot{\theta}_i \\ \vdots \end{Bmatrix} + \begin{Bmatrix} \vdots \\ \dot{\theta}_i \\ \vdots \end{Bmatrix} = \begin{bmatrix} \ddots & \\ & K_i \\ & & \ddots \end{bmatrix} \left[A \right]^{-1} \begin{Bmatrix} \vdots \\ C_D - C_A \\ \vdots \end{Bmatrix} \tag{34}$$

Where τ_i are time constants (to filter out oscillatory inputs), θ_i are the controls, K_i are gains, $[A]$ is a matrix of control couplings, C_A are computed trim variables, and C_D are the desired values of C_A. A crucial step in understanding these equations is to understand that C_A is related to the controls in the following way

$$\{C_A\} = \{C_A\}_0 + [B]\{\theta_i\} \tag{35}$$

Thus, the closed-loop control equations become

$$\begin{bmatrix} \ddots & \\ & \tau_i \\ & & \ddots \end{bmatrix} \begin{Bmatrix} \vdots \\ \ddot{\theta}_i \\ \vdots \end{Bmatrix} + \begin{Bmatrix} \vdots \\ \dot{\theta}_i \\ \vdots \end{Bmatrix} + \begin{bmatrix} \ddots & \\ & K_i \\ & & \ddots \end{bmatrix} \left[A \right]^{-1} \left[B \right] \begin{Bmatrix} \vdots \\ \theta_i \\ \vdots \end{Bmatrix} =$$

$$\begin{bmatrix} \ddots & \\ & K_i \\ & & \ddots \end{bmatrix} \left[A \right]^{-1} \begin{Bmatrix} \vdots \\ C_D - C_{A0} \\ \vdots \end{Bmatrix} \tag{36}$$

In past studies (and this present one), the controller is designed such that $[A]$ is taken to be as close to $[B]^{-1}$ as possible. When this is done exactly, the homogeneous equations for each control become uncoupled,

$$\tau_i \overset{**}{\theta}_i + \overset{*}{\theta}_i + K_i \theta_i = 0 \tag{37}$$

This gives a natural frequency $\omega_n = \sqrt{K_i/\tau_i}$, a damping ratio $\zeta = 1/(2\sqrt{K_i \tau_i})$, and a settling time $t_s = 1.46/K_i$ (revolutions) for $\zeta < 1$. It is clear that an optimum controller would have infinite gain. However, there are actually higher-order blade dynamics implicit in the B matrix that are not included in the approximation of Eq. (35) nor in the quasi-steady $[A]$ couplings. Thus, large K can drive the system unstable. Therefore, optimum designs have tended to increase K to near the stability boundary and then to pick τ large enough to filter out oscillatory response but small enough to keep ω_n around .25 to .33 (3 to 4 rotor revolutions per controller cycle).

Nevertheless, despite these fairly successful efforts, oscillations in final control settings have not been completely satisfactory due to the fact that only a single blade is modeled, which gives large $2/rev$ oscillations in C_T (θ_0) and large $1/rev$ oscillations in C_L and C_M (θ_s and θ_c). To solve this problem, we have, by taking information from past time history as "other" blades, modified the controller to assume that Q blades are present. Thus, rather than feeding back $C_A(\bar{t})$, we feed back

$$\bar{C}_A(\bar{t}) = \frac{C_A(\bar{t}) + C_A(\bar{t} - \frac{2\pi}{Q}) + C_A(\bar{t} - 2\frac{2\pi}{Q}) + \cdots + C_A(\bar{t} - \frac{Q-1}{Q} 2\pi)}{Q} \tag{38}$$

This essentially filters out from C_A all harmonics not integer multiples of Q . However, it also introduces additional time delays into the system. For example, for $Q = 2$, if we use the Padé approximate to the time delay, we obtain for the homogeneous equation

$$\frac{\pi}{2} \overset{***}{\theta}_i + (\tau_i + \frac{\pi}{2}) \overset{**}{\theta}_i + \overset{*}{\theta} + K\theta_i = 0 \tag{39}$$

Thus, there is a higher-order $\overset{***}{\theta}$ term (negligible for small values of ω_n) and an added $\pi/2$ on the $\overset{**}{\theta}$ term. In general, for Q blades, the equivalent total τ on the $\overset{**}{\theta}$ term is,

$$\tau_{eq} = \frac{Q-1}{Q}\pi + \tau_i \tag{40}$$

In the limit as Q goes to infinity, we can define the limit of Eq. (38)

$$\bar{C}_A = \frac{1}{2\pi} \int_{\bar{t}-2\pi}^{\bar{t}} C_A(t) dt \tag{41}$$

Thus, for $\tau_i = 0$ and $Q = \infty$, we have $\tau_{eq} = \pi$ which is about the optimum from previous work. Thus, for $Q = \infty$, the $\overset{**}{\theta}$ term could be removed Eq. (34).

$$\begin{Bmatrix} \vdots \\ \overset{*}{\theta}_i \\ \vdots \end{Bmatrix} = \begin{bmatrix} \ddots & & \\ & K_i & \\ & & \ddots \end{bmatrix} \begin{bmatrix} A \end{bmatrix}^{-1} \begin{Bmatrix} \vdots \\ C_D - C_A \\ \vdots \end{Bmatrix} \tag{42}$$

Fig. 4 shows the settling time for such a controller as a function of gain, $K_0 = K_1$. (Discontinuities occur when the settling time moves off of a given peak to a new peak.) Thus, the optimum gain is about .15. However, as we shall see, when additional unmodeled dynamics enter the problem, K must be reduced for stability. In the work below, we use the $Q = 2$ controller so that the $\overset{**}{\theta}$ term must be retained, with a small added time-constant, τ_i. We have found that the $Q = 2$ controller: 1) filters out all unwanted control oscillations, 2) is easy to program, and 3) allows more flexibility in the choice of τ_{eq}.

4 Results

4.1 Solution Method

In this section, approximate solution methods are applied to the elastic Eqs. (1), (3), and (5), then combined with Eqs. (33). The aerodynamic circulations are expressed by Eqs. (11), (12), and (17). Only lower order terms of this equations are to be considered in the following analyses in order to reduce complexity. This allows the investigation of the general trends of the results, without going into cumbersome computation.

The application of the Ritz-Galerkin procedure transforms the flap, lag, and torsion Eqs. (1), (3), and (5) to ordinary differential equations. The coefficients of the equations have integral forms which can be determined after selection of comparison functions. These coefficients are presented in Ref. [16]. The resultant equations are:
Flap equation

$$\sum_{j=1}^{N} I_{ij}^{6} \ddot{q}_j + \sum_{j=1}^{N} (I_{ij}^{10} + \Lambda_2 I_{ij}^{8} + \bar{K}_\beta B_{ij}^{1}) q_j = \frac{\gamma}{6a} \sum_{l=1}^{M} (\bar{\Gamma}_{1l} + \bar{\Gamma}_{2l})(\mu \sin\psi I_{il}^{4} + I_{il}^{5}) \tag{43}$$

Lag equation

$$\sum_{j=1}^{N} J_{ij}^{6} \ddot{p}_j + \sum_{j=1}^{N} (J_{ij}^{10} - J_{ij}^{6} + \Lambda_1 J_{ij}^{8} + \bar{K}_\zeta B_{ij}^{1}) p_j - 2 \sum_{j=1}^{N} \sum_{k=1}^{N} I_{ijk}^{13} \dot{q}_k q_j$$

$$+(\Lambda_1 - \Lambda_2)(\theta + \phi) \sum_{j=1}^{N} J_{ij}^{8} q_j = -\frac{\gamma}{6a} \sum_{j=1}^{N} \sum_{l=1}^{M} (\bar{\Gamma}_{1l} + \bar{\Gamma}_{2l}) \{ J_{ijl}^{12} \mu \cos\psi q_j + J_{ijl}^{11} \dot{q}_j$$

$$+\alpha_c \mu J_{il}^{4} + (\frac{4}{3}\nu_0 + \nu_c \cos\psi) J_{il}^{5} \} + C_D \frac{\gamma}{6a} (J_i^3 + 2\mu \sin\psi J_i^2 + \mu^2 \sin^2\psi J_i^1) \tag{44}$$

Torsion equation

$$\sum_{j=1}^{N} \bar{k}_m^2 I_{ij}^{16} \ddot{r}_j - \frac{1}{6} \frac{\gamma \bar{c}^2}{a} c_1 \sum_{j=1}^{N} (I_{ij}^{17} + \mu \sin\psi I_{ij}^{16}) \dot{r}_j$$

$$+ \sum_{j=1}^{N} (\bar{K}_\phi B_{ij}^{2} + \Lambda_3 \bar{J} I_{ij}^{18} - \frac{1}{12} \frac{\gamma \bar{c}^2}{a} c_1 \mu \cos\psi I_{ij}^{16}) r_j =$$

$$\frac{1}{6} \frac{\gamma \bar{c}}{a} \{ \sum_{l=1}^{M} (C_{mLl} + C_{m2l}) [I_{il}^{24} + 2\mu \sin\psi I_{il}^{23} + (\mu \sin\psi)^2 I_{il}^{22}]$$

$$+c_1 \bar{b} [(2\dot{\theta} + \nu_c \sin\psi) I_i^{15} + \mu (2\dot{\theta} \sin\psi + \theta \cos\psi) I_i^{14}]$$

$$+c_1 \bar{b} \sum_{j=1}^{N} [-\mu \cos\psi I_{ij}^{20} \dot{q}_j + (I_{ij}^{21} + 2\mu \sin\psi I_{ij}^{20}) q_j - I_{ij}^{19} \ddot{q}_j] \} \tag{45}$$

where the induced velocity is assumed to be $\bar{V}_i = \alpha_c \mu + 4/3 \nu_0 \bar{x} + \nu_c \bar{x} \cos\psi$. After selection of N comparison functions, it is possible to compute the coefficients of the above equations. This results in 3N linear differential equations to be solved for the generalized coordinate in time domain.

Before moving to the aerodynamic equations, it is convenient to discuss the selection of comparison functions required for the above equations. The results obtained in this section are based on the rigid blade assumption. This approximation is used in the early stages of this work in order to validate the aeroelastic model and to trace its efficiency and drawbacks in less complicated cases. An elastic blade may be treated in

Table 3: Baseline Parameters

Parameter	Numerical Value	Physical Description
γ	6.63	Lock number
a	6.461	lift curve slope
C_D	0.01	drag coefficient
Λ_1	0.014	$\frac{EI_y}{m\Omega^2R^4}$
Λ_2	0.002	$\frac{EI_x}{m\Omega^2R^4}$
$\bar{b}$	0.05	$\frac{b}{R}$
p	1.03	flap frequency
f	0.01	flat plate drag
σ	0.1	solidity
K_β	0.0203	stiffness of flap root
K_ζ	0.02083	stiffness of lag root
C_ζ	0.025	damping coefficient
τ_0	2.94	time constant
τ_1	.31	time constant
K_0	.27	gain
K_1	.18	gain

a similar manner, but more degrees of freedom need to be included. This implies more equations to be solved because of the extra degrees of freedom.

Table 3 gives the common parameters used in the cases discussed in this section. These parameters are selected from current helicopter data and used for illustration purposes. The drag coefficient is assumed constant in the work presented here. The authors have already reviewed a few nonlinear drag models and implemented them for simple problems. In future work, we intend to include a nonlinear drag model and to include a variable C_D based on the stall assumption. The study conducted so far concentrates on the effect of stall on lift but not on drag. The controller gains and time constants were chosen from a formal optimization procedure applied to linear, rigid-blade flapping equations at $\mu = 0.3$.

4.2 Steady State Response

The determination of the steady state response of rotor blades is necessary for the prediction of loads and vibrations. The differential equations describing the blade response are integrated in time until all the transients have died out and a periodic and trimmed response is obtained. A case is considered to be trimmed when the control settings θ_0, θ_s, and θ_c reach stable positions. The control angles are thought of as converged when they reach a value within +/- 0.5 degree of their final value in a limited number of cycles. Here, the integration is limited to 24 cycles to avoid unreasonnable computational cost. The trim procedure supresses the first harmonic vibrations of the flap response through the $Q = 2$ time delay.

The flap and lag angles are set initially to zero. The initial values of the control settings, on the other hand, are computed using approximate trim equations. This method allows a resonable initial guess of the controllers which reduces the convergence time.

Results have been obtained for a variety of advance ratios and thrust coefficients. The results are given for the twenty-fourth revolution. Though the majority of cases converge in less than ten cycles, it takes longer for those conditions close to the convergence boundaries of the controller.

4.3 Effect of Advance Ratio

Advance ratio is the normalized free stream velocity with respect to the blade tip speed. At high advance ratios, the retreating blade encounters large angles of attack. This causes a region of the rotor to enter the stall regime. We will now present rotor response for four moderate to high values of advance ratio at a constant thrust coefficient, $C_T = 0.01$. A single C_T is chosen so that it illustrates the response at the trim boundaries. The convergence speed becomes slower as the advance ratio increases. Fig. 5 gives time histories of the control angle, θ_0. Ideally, the control settings should reach a steady state. At an advance ratio of $\mu = 0.38$, large once per-rev oscillations start to have a significant effect on the controllers. Also, the amplitude of the response becomes larger; and the convergence rate is poor. At higher advance ratio, these effects take a more significant role. Smoothly converging response becomes impossible.

The contribution of a single blade section to the total lift is plotted versus its local angle of attack, Fig. 6. The figure shows a hysteresis loop, typical of dynamic stall. Large negative angles of attack can occur at the most inboard element due to reversed flow. This element, however, has a positive angle of attack along the total revolution.

4.4 Effect of Thrust on Trim

Rotor response may be effected considerably by stall either when the advance ratio increases or when the gross weight is increased for the same rotor. Fig. 7 illustrates the time history of the control response for a constant advance ratio, $\mu = 0.3$, and various values of the thrust coefficient. As the thrust coefficient increases, the convergence becomes slower and the effect of the once-per-rev component appears more significant. At a thrust coefficient of $C_T = 0.015$, the convergence is very slow compared to the other cases. Fig. 8 shows the limits of C_T and μ for which the rotor can be trimmed. The dashed curve is with the hover control couplings, $[A_0]^{-1}$, and the solid line is for the more accurate couplings, $[A_\mu]^{-1}$. The main effect of improved couplings is to shift the trim limits from $\mu = 0.4$ to $\mu = 0.6$. There is much less change on the C_T boundary. This implies that the C_T boundary may be a physical limitation to trim rather than a numerical limit.

In Figs. 9-11, the control settings are plotted as functions of the advance ratio for various thrust levels both for the complete dynamic stall model and for a linear aerodynamic model. The later model is similar to the former one but the nonlinear aerodynamic component is ignored in the later. Thus, it is a linear aerodynamic model in which the linearity continues even beyond the critical angle of attack. The collective pitch, θ_0, decreases to a minimum due to induced flow effects and then increases slowly as the advance ratio reaches higher values. This variation is in conjunction with the typical variation of the power required with cruise speed. On the other hand, the cyclic pitch is zero at hover, $\mu = 0$. This is because of the symmetry of the blade coning at hover. The longitudinal cyclic pitch, θ_s, increases in magnitude with advance ratio to account for the loss of free-speed velocity on the retreating blade. The lateral cyclic pitch, θ_c, is associated with the trim of aerodynamic coupling due to coning. Thus, it increases until it reaches a nearly stationary value.

For low values of thrust coefficients, both models predict the same control set-

tings. At high loadings, such as $C_T = 0.014$, the controls have higher values when stall is modeled. In particular, the longitudinal cyclic pitch increases more significantly at the begining of the stall regime. This is because the loss of lift is more pronounced in the neighborhood of $\psi = 270^0$. For $\mu = 0.35$, the response is close to trim but not fully trimmed.

4.5 Effect of Torsion on Trim

When the torsional degree of freedom and elastic modes are included in the aeroelastic model, the controller, with the previous gains and time constants ($\tau_0 = 2.94$, $\tau_1 = .31$, $K_0 = .27$, $K_1 = .18$) fails to attain a trimmed condition for torsional frequencies lower than $8/rev$. This failure occurs for any choice of advance ratio μ and thrust coefficient C_T. Torsional deflections enter into the blade dynamics through a variable torsionl angle (for an elastic blade) which is added to the blade pitch. High torsional frequency corresponds to a blade with high torsional rigidity for which the effect of torsion is not important. A blade which is torsionally soft, however, causes the torsional defections to have a more significant effect on the controller. Therefore, the trimming errors were examined at low torsional frequencies. This examination revealed large oscillations in these errors. Since the system stability depends directly on the cyclic gains, these gains have been lowered to a K_1 value of 0.05. The new choice of gains allows the controller to trim successfully for torsional frequencies as low as $5/rev$. However, for torsional frequencies lower than $5/rev$, numerical experiments with gains do not bring any significant improvement to trim. Thus, an adaptive $[A] = [B]^{-1}$ may be required.

The collective and cyclic pitch produced by the low-gain controller are shown in Figs. 12-14. The torsional angle is shown in Fig. 15. Several observations can be drawn from these figures. First, the variation of the torsional deflection agrees with the physical expectation. Both the average and the oscillatory amplitude of torsional deflections increase as the torsional frequency decreases. Since this average is negative, the collective pitch must increase, Fig. 12, in order to maintain the desired lift. Similarly, the longitudinal and lateral pitch angles decrease for lower freqencies. This is due to the fact that torsional deflection oscillations are domminated by once-per-rev oscillations.

In addition, numerical experiments and theoretical observations confirm that a trimmed condition for low torsional frequencies cannot be achieved by a simple adjustment of the gains and time constants, since some approximations are inherit in the auto-pilot couplings. One approximation is the neglect of the torsional deflection in the angle-of-attack expression used during the derivation of the coupling matrix. Thus, as these deflections play a more important role, the coupling matrix may have to include the effect of torsion. Though approximate theoritical methods may lead to the addition of the effect of torsion to the coupling matrix, an adaptive numerical method may be necessary for the general case. For more details, the reader is referred to Ref. [16].

5 Conclusions

A more general rotor auto-pilot has been developed that can be used to control any number of trim variables. Although it can be applied to rotors with an arbitrary number of blades, it is most often applied to a single blade, with other blades simulated through time delay functions. In this case, optimum gain is about $.05 - .18$ with the maximum value determined by stability of higher-order dynamics. The equivalent time constant for best results is about π/Q.

The state-space stall model is a viable means of accounting for dynamic stall,

and stall does not seem to affect the controller adversely. However, torsional frequencies below $5/rev$ cause controller instability at any gain. It is suggested that an adaptive controller be used which could result in stable trim at all values of thrust and advance ratio, and with elastic blade dynamics.

Acknowledgement

The development of the optimized controller was sponsored by Interdisciplinary Research Division, NASA Langley Research Center, Grant No. NAG-1-710, Howard Adelman, technical monitor. The development of the state-space stall model and the flap-lag-torsion modeling were performed in the Georgia Tech Center of Excellence for Rotary-Wing Aircraft Technology under Army Research Office Funding, Robert Singleton, Technical Monitor.

References

1. Panda, B. and Chopra I., "Flap-Lag-Torsion Stability in Forward Flight," *Journal of the American Helicopter Society*, Vol. 30, No. 4, Oct. 1985, pp. 30-39.

2. Peters, D.A. and Ormiston, R., "Flapping Response Characteristics of Hingless Rotor Blades by a Generalized Harmonic Balance Method," NASA TN D7856, February 1975.

3. Friedmann, P.P. and Kottapalli S.-B.-R., "Coupled Flap-Lag-Torsional Dynamics of Hingeless Rotor Blades in Forward Flight," *Journal of the American Helicopter Society*, Vol. 27, No. 4, Oct. 1982, pp. 28-36.

4. Peters, D.A and Izadpanah, A., "Helicopter Trim by Periodic Shooting with Newton-Raphson Iteration," *Proceedings of the 37th Annual National Forum of the American Helicopter Society*, New Orleans, Louisiana, May 1981, Paper 81-23.

5. Eipe, A., *Effect of Some Structural Parameters on Elastic Rotor Loads by an Iterative Harmonic Balance*, Doctor of Science Thesis, Washington University, Dec. 1979.

6. Peters, D.A., Kim, B.S., and Chen, H.-S, "Calculation of Trim Settings of a Helicopter Rotor by an Optimized Automatic Controller," *Journal of Guidance, Control, and Dynamics*, Vol. 7, No. 1, Jan.-Feb. 1984, pp. 85-91.

7. Friedmann, P.P. and Venkatesan, C., "Finite State Modeling of Unsteady Aerodynamics and Its Application to a Rotor Dynamic Problem," *Proceedings of the 11th European Rotorcraft Forum*, London, England, Sept. 10-13, 1985, Paper No. 72.

8. Johnson, W., "General Time-Domain Unsteady Aerodynamic of Wings," *Proceedings of the 25th Aircraft Symposium of Japan Society for Aeronautical and Space Sciences*, Tokyo, December 14-16, 1987.

9. Peters, D.A. and He, C.J., "Comparison of Measured Induced Velocities With Results From a Closed-Form Finite State Wake Model in Forward Flight," *Proceedings of the 45th Annual National Forum of the American Helicopter Society*, Boston, Massachusetts, May 22-24, 1989.

10. Elliott, A.S., *Calculation of the Steady Periodic and Gust Response of a Hingless Rotor Helicopter Using Two-Dimensional Time Domain Unsteady Aerodynamics*, Doctor of Science Thesis, University of Maryland, 1987.

11. Tran, C. T. and Petot, D., "Semi-Empirical Model for the Dynamic Stall of Airfoils in View of the Application to the Calculation of Responses of a Helicopter Blade in Forward Flight," *Vertica*, Vol. 6, 1982, pp. 219-239.

12. Peters, D.A, "Toward a Unified Lift Model for Use in Rotor Blade Stability Analysis," *Journal of the American Helicopter Society*, Vol. 30, No. 3, July 1985, pp. 32-42.

13. Petot, D. and Dat, R., "Unsteady Aerodymic Loads on an Oscillating Airfoil with Unsteady Stall," *Proceedings of the Helicopter Research Work-Shop,* Boca Raton, Florida, November 1987.

14. Peters, D. and Chouchane, M., "Effect of Dynamic Stall on Helicopter Trim and Flap-Lag Response," *Journal of Fluids and Structures*, Vol. 1, 1987, pp. 299-318.

15. Karunamoorthy, S. N. and Peters, D. A., "Use of Hierarchical Elastic Blade Equations and Automatic Trim For Rotor Response," *Vertica*, Vol. 11, 1987, pp. 233-248.

16. Chouchane, M. *Application of a Dynamic Stall Model to Rotor Trim and Aeroelastic Response,* Doctor of Science Thesis, Georgia Institute of Technology, Aug. 1989.

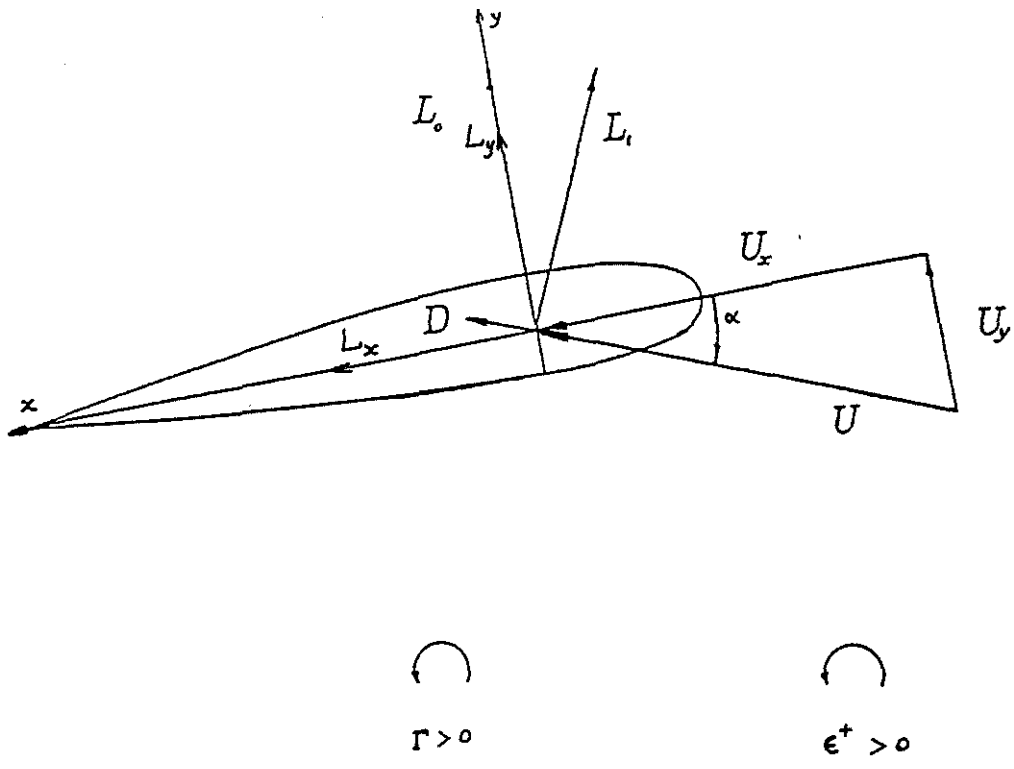

Figure 1: Aerodynamic Forces in the Deformed Blade Coordinate System.

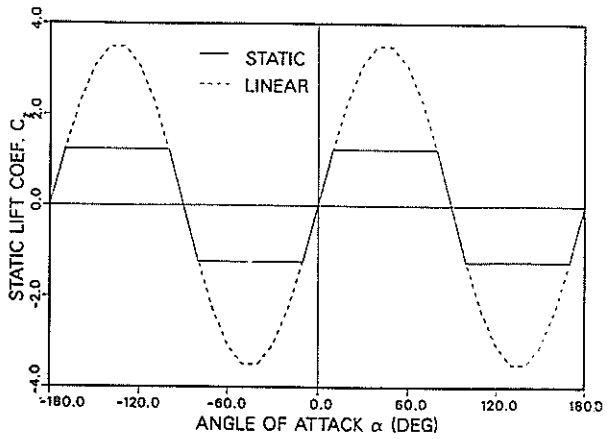

Figure 2: Static and Linear Lift Coefficients vs Angle of Attack

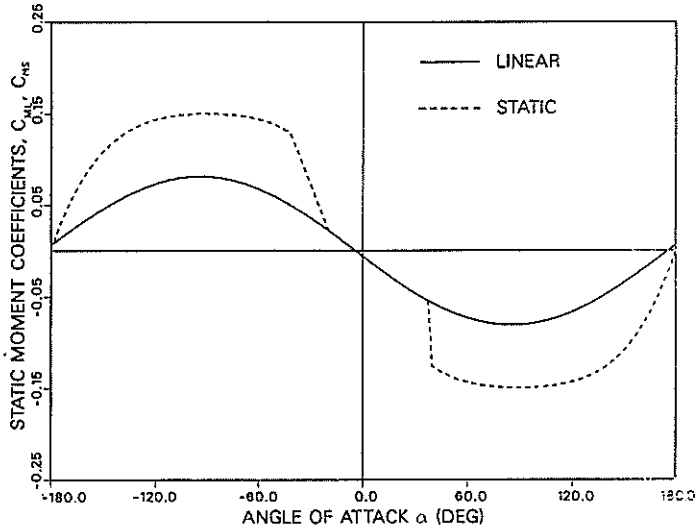

Figure 3: Static and Linear Moment Coefficients vs Angle of Attack

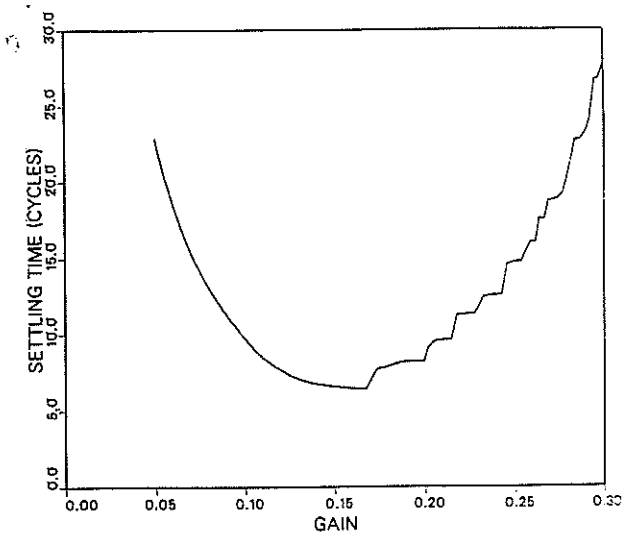

Figure 4: Settling Time vs Gain

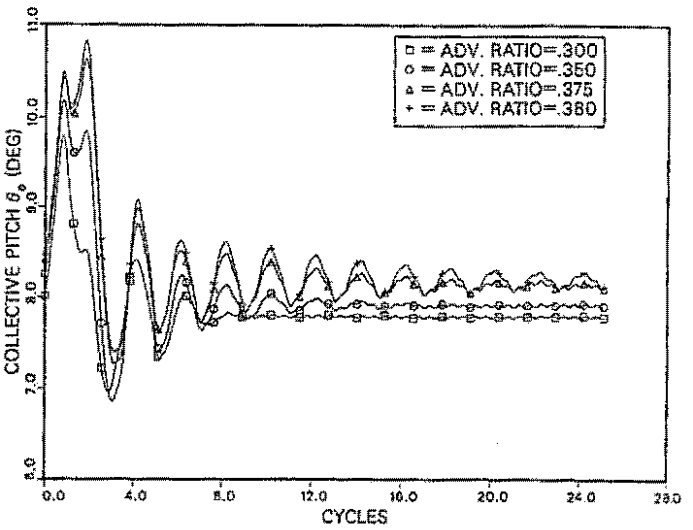

Figure 5: Collective Pitch vs Cycles of Rotation @ $C_T = 0.01$

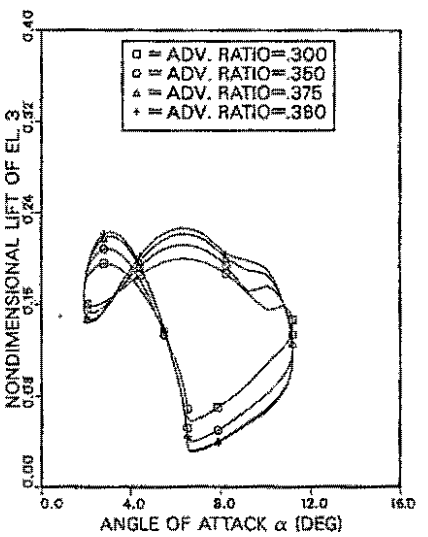

Figure 6: Nondimensional Lift of Element 3 vs Angle of Attack @ $C_T = 0.01$

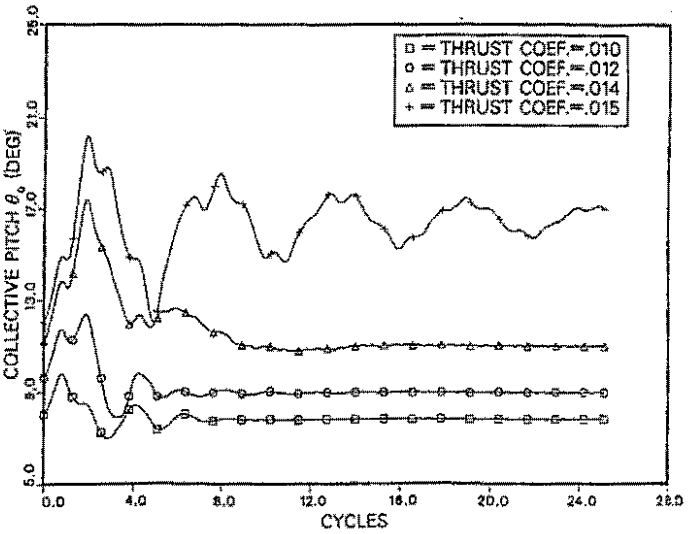

Figure 7: Collective Pitch vs Cycles of Rotation @ $\mu = 0.30$

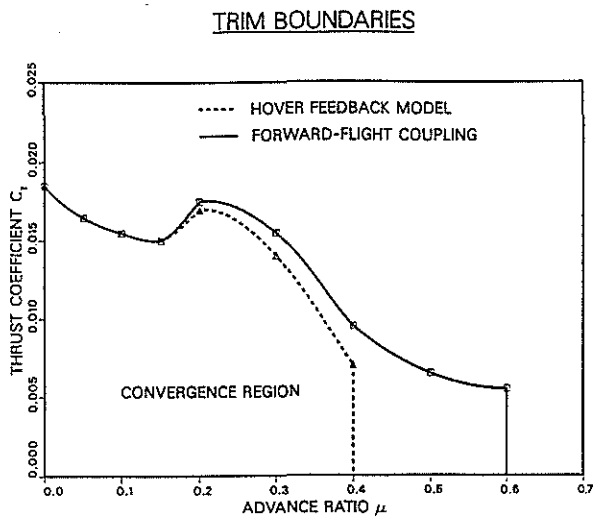

Figure 8: Trim Boundaries for Two Control Cases

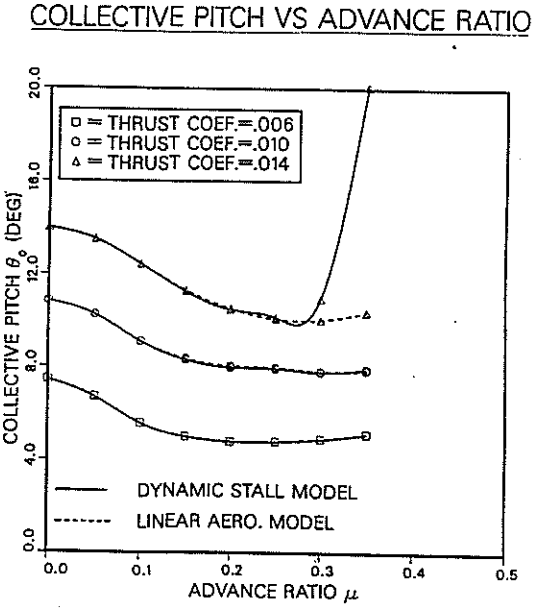

Figure 9: Collective Pitch vs Advance Ratio

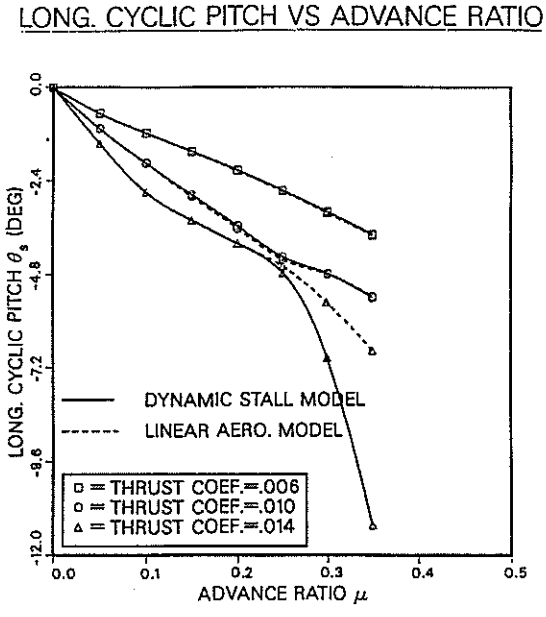

Figure 10: Longitudinal Cyclic Pitch vs Advance Ratio

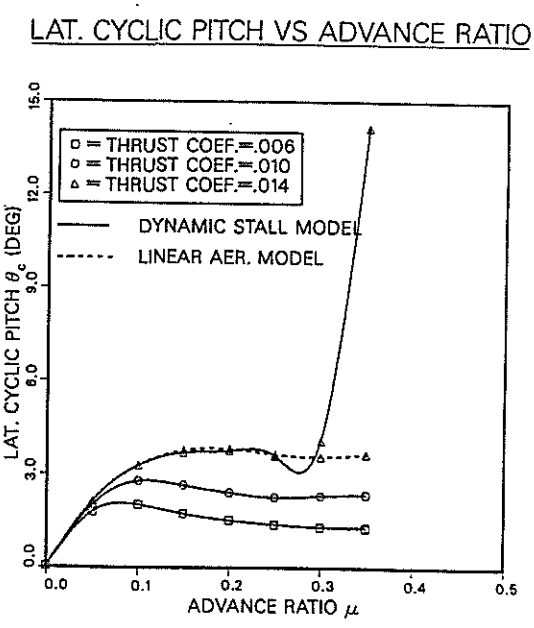

Figure 11: Lateral Cyclic Pitch vs Advance Ratio

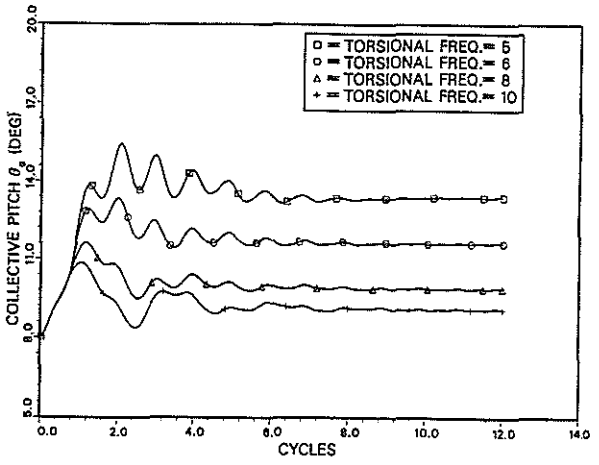

Figure 12: Collective Pitch vs Cycles of Rotation @ $C_T = 0.01$ and $\mu = 0.30$

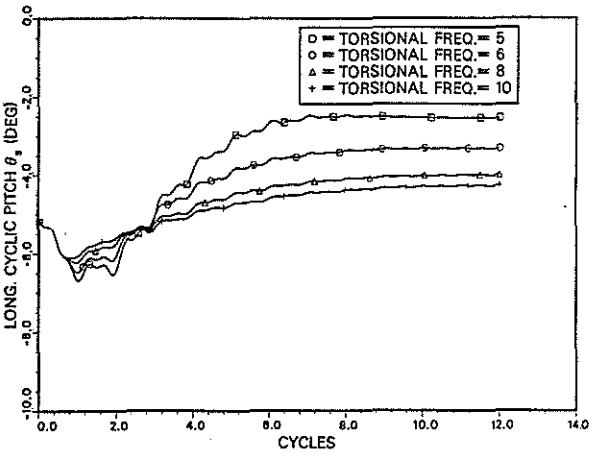

Figure 13: Longitudinal Cyclic Pitch vs Cycles of Rotation @ $C_T = 0.01$ and $\mu = 0.30$

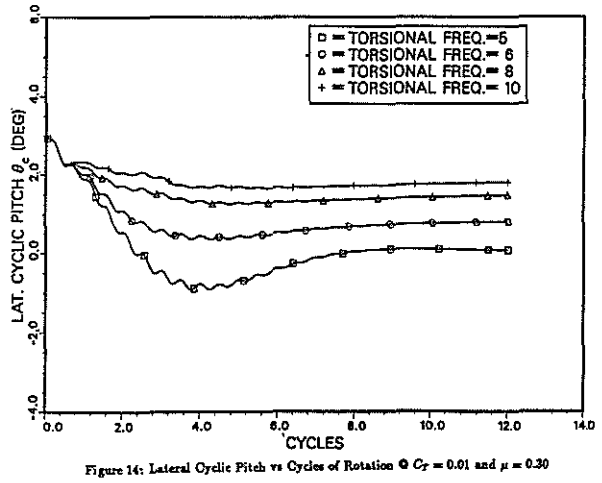

Figure 14: Lateral Cyclic Pitch vs Cycles of Rotation @ $C_T = 0.01$ and $\mu = 0.30$

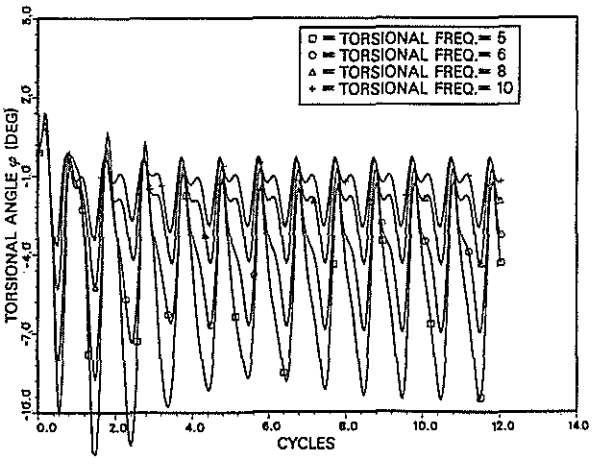

Figure 15: Torsional Deflection vs Cycles of Rotation @ $C_T = 0.01$ and $\mu = 0.30$